Computers & Geosciences 100 (2017) 76–86

Contents lists available at ScienceDirect

Computers & Geosciences

journal homepage: www.elsevier.com/locate/cageo

Research paper

Development of a coupled wave-flow-vegetation interaction model

Alexis Beudin, Tarandeep S. Kalra, Neil K. Ganju*, John C. Warner

US Geological Survey, Woods Hole, MA 02543, USA

ARTICLE INFO

Keywords:
Flexible aquatic vegetation
Coastal hydrodynamics
Numerical modeling

ABSTRACT

Emergent and submerged vegetation can significantly affect coastal hydrodynamics. However, most deterministic numerical models do not take into account their influence on currents, waves, and turbulence. In this paper, we describe the implementation of a wave-flow-vegetation module into a Coupled-Ocean-Atmosphere-Wave-Sediment Transport (COAWST) modeling system that includes a flow model (ROMS) and a wave model (SWAN), and illustrate various interacting processes using an idealized shallow basin application. The flow model has been modified to include plant posture-dependent three-dimensional drag, in-canopy wave-induced streaming, and production of turbulent kinetic energy and enstrophy to parameterize vertical mixing. The coupling framework has been updated to exchange vegetation-related variables between the flow model and the wave model to account for wave energy dissipation due to vegetation. This study i) demonstrates the validity of the plant posture-dependent drag parameterization against field measurements, ii) shows that the model is capable of reproducing the mean and turbulent flow field in the presence of vegetation as compared to various laboratory experiments, iii) provides insight into the flow-vegetation interaction through an analysis of the terms in the momentum balance, iv) describes the influence of a submerged vegetation patch on tidal currents and waves separately and combined, and v) proposes future directions for research and development.

1. Introduction

Aquatic vegetation (e.g., mangroves, salt marshes, and seagrasses) plays an important role in estuarine ecosystems by acting as a seabed stabilizer, nutrient sink, and nursery for juvenile fishes and invertebrates (Hemminga and Duarte, 2000). They are often referred to as eco-engineers because they modify their physical environment to create more favorable habitat for themselves and other organisms (Jones et al., 1994). For example, seagrasses can reduce sediment resuspension thereby increasing light penetration and potential growth (Carr et al., 2010). Evaluating the resilience of estuarine ecosystems requires greater insight into the interactions between vegetation, currents, waves, and sediment transport. The relevance of aquatic vegetation in coastal protection from extreme events has become a recurring question along with the viability assessment of ecosystem-based management approaches (Barbier et al., 2008; Temmerman et al., 2013).

Previous laboratory and numerical investigations have focused on the blade-to-meadow scale (detailed review by Nepf, 2012). Paired with theoretical analysis, they stand as valuable tools to study vegetated flow dynamics (Fig. 1). However, they do not consider the inherent complexity of realistic environments (e.g., spatial variations of vegetation distribution and bathymetry, nonlinear wave-current interactions). Coastal ocean numerical models can be used to investigate these complex processes, but their resolution often requires parameterizations to account for small (sub-grid) scale turbulent features of the flows, which are particularly important in the presence of vegetation.

The simplest method to account for the influence of vegetation in a depth-averaged flow model is an increase of the bottom roughness coefficient (Ree, 1949; Morin et al., 2000). More recently, vegetation has been parameterized as a source of form drag as opposed to skin friction relevant to sediment transport in the depth-averaged sense (Chen et al., 2007; Le Bouteiller and Venditti, 2014). However, two-dimensional depth-averaged (2DH) approximations cannot account for the complex vertical structure of the flow within and over submerged vegetation (Sheng et al., 2012), especially shear layers at the top of the canopy that enhance vertical mixing (Lapetina and Sheng, 2014; Marjoribanks et al., 2014). To date, few estuary-scale models account for the three-dimensional influence of vegetation on the mean and turbulent flow (Temmerman et al., 2005; Kombiadou et al., 2014; Lapetina and Sheng, 2015), and none are part of an open-source, community model. In addition to exerting drag on the mean flow, aquatic vegetation also attenuates waves. While the bed-roughness approach has been rather successfully applied to simulate wave height decay over vegetation (Möller et al., 1999; de Vriend, 2006; Chen et al.,

* Corresponding author.
E-mail address: nganju@usgs.gov (N.K. Ganju).

http://dx.doi.org/10.1016/j.cageo.2016.12.010
Received 16 May 2016; Received in revised form 18 August 2016; Accepted 14 December 2016
Available online 15 December 2016
0098-3004/ Published by Elsevier Ltd.

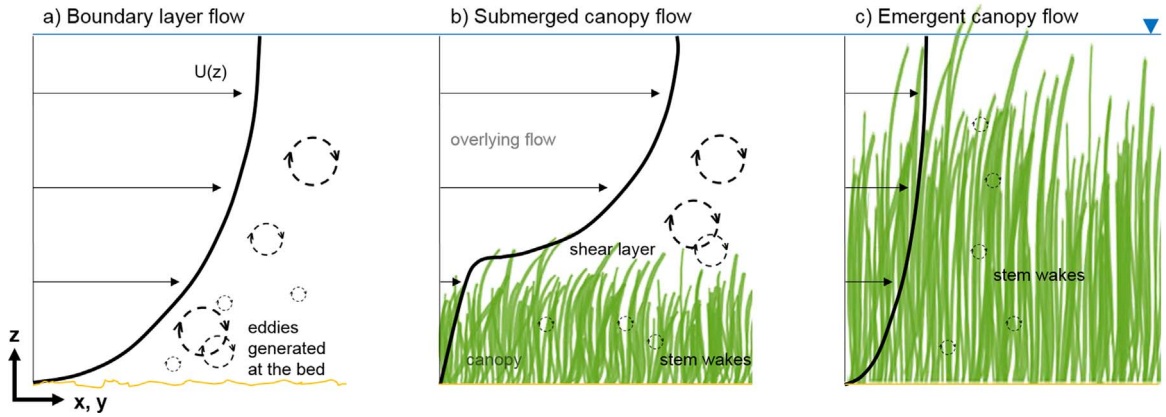

Fig. 1. Sketch of three different flow regimes. The dominant source of turbulence is respectively (from left to right) the bed, the top of the canopy (shear layer), and the stem wakes.

2007), the cylinder approach of Dalrymple et al. (1984) provides a more physically based description of wave dissipation by vegetation and its implementation in spectral wave models has been validated against flume experiments (Mendez and Losada, 2004; Suzuki et al., 2012; Wu, 2014; Bacchi et al., 2014).

The present study aims at providing an open-source process-based modeling framework that allows comprehensive studies of the interactions between hydrodynamics and vegetation, and describing/illustrating the influence of a submerged vegetation patch on currents and waves in an idealized shallow basin. We first detail the implementation of flow-vegetation interaction processes within the models, and then assess the model results using prior studies. We detail the interaction between flow and vegetation for a number of idealized cases, then discuss future avenues of model application and improvement.

2. Methods

The wave-flow-vegetation module described in this paper is implemented as part of the open-source Coupled Ocean-Atmosphere-Wave-Sediment Transport (COAWST) numerical modeling system (Warner et al., 2010), operating on the flow (ROMS) and wave (SWAN) models (Fig. 2) coupled via the Model Coupling Toolkit (MCT) generating a single executable program (Warner et al., 2008a, 2008b). The vegetation parameterizations are successively described in the flow and wave models.

2.1. Flow model

ROMS (Regional Ocean Modeling System) is a three-dimensional,

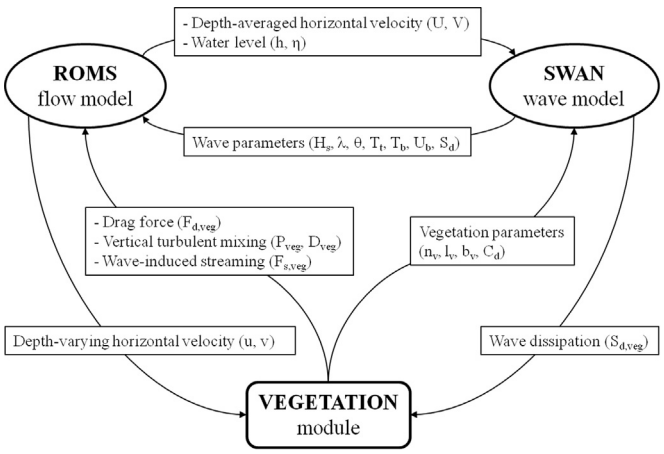

Fig. 2. Diagram showing data exchanges between the flow model, the wave model, and the vegetation module in COAWST.

free surface, finite-difference, terrain-following model that solves the Reynolds-Averaged Navier-Stokes (RANS) equations using the hydrostatic and Boussinesq assumptions (Haidvogel et al., 2008):

$$\frac{\partial u}{\partial t}+\vec{v}\bullet\nabla u-fv=-\frac{\partial \phi}{\partial x}-\frac{\partial}{\partial z}\left(\overline{u'w'}-\nu\frac{\partial u}{\partial z}\right)+D_u+F_u \tag{1a}$$

$$\frac{\partial v}{\partial t}+\vec{v}\bullet\nabla v+fu=-\frac{\partial \phi}{\partial y}-\frac{\partial}{\partial z}\left(\overline{v'w'}-\nu\frac{\partial v}{\partial z}\right)+D_v+F_v \tag{1b}$$

$$-\frac{\partial \phi}{\partial z}-\frac{\rho g}{\rho_0}=0 \tag{1c}$$

$$\frac{\partial u}{\partial x}+\frac{\partial v}{\partial y}+\frac{\partial w}{\partial z}=0 \tag{1d}$$

where (u,v,w) are the velocity vector $\vec{v}$ components in the horizontal (the Cartesian coordinates x and y can be replaced by more general curvilinear coordinate ξ and η, in which case additional metric terms appear in the equations) and vertical (z is actually scaled to sigma-coordinate) directions respectively, f is the Coriolis parameter, ϕ is the dynamic pressure (normalized by the reference density of seawater ρ_0), ρ is the density, ν is the molecular viscosity, (D_u, D_v) are the horizontal diffusive terms calculated with the vector Laplacian of the velocity field, and (F_u, F_v) are the forcing terms that include wave-averaged forces (Kumar et al., 2012) and vegetation drag force and in-canopy wave-induced streaming (described in the next paragraphs).

The (spatially averaged) vegetation drag force can be approximated using a quadratic drag law:

$$F_{d,\ veg,u}=\frac{1}{2}C_D b_v n_v u\sqrt{u^2+v^2} \tag{2a}$$

$$F_{d,\ veg,v}=\frac{1}{2}C_D b_v n_v v\sqrt{u^2+v^2} \tag{2b}$$

where ρ is the (total) density of seawater, C_D is the plant drag coefficient (constant assuming a high Reynolds number), b_v is the width of individual plants, n_v is the number of plants per unit area, and (u,v) are the horizontal velocity components at each vertical level in the canopy of height l_v (when upright). A limiter is imposed to prevent the vegetation drag force from having a value large enough to reverse the velocity direction (see also bottom stress limiter due to wetting and drying in Warner et al., 2013).

To quantify the reduction of drag due to the bending of flexible plants, Dijkstra (2012) implemented a lookup table of deflected height and equivalent drag coefficient based on a detailed one-dimensional vertical model of plant motion called Dynveg (Dijkstra and Uittenbogaard, 2010), while Kombiadou et al. (2014) used an empirical formula based on laboratory data of Ganthy (2011) for the height of the bent canopy. In the present study, the more generally applicable (across vegetation species and hydrodynamic conditions) approach of

Luhar and Nepf (2011) has been implemented. An effective blade length (l_{ve}) is defined as the length of a rigid vertical blade that generates the same horizontal drag as the flexible blade of total length (l_v), accounting for drag reduction both due to the reduced frontal area (deflected height times width) and to the more streamlined shape of the bent blades. Based on a theoretical plant posture model (described in details in Luhar and Nepf, 2011), the effective blade length expression can be reduced to (Eq. (16) in Luhar and Nepf, 2011):

$$\frac{l_{ve}}{l_v}=1-\frac{1-0.9Ca^{-1/3}}{1+Ca^{-3/2}(8+B^{3/2})} \tag{3a}$$

where Ca is the Cauchy number and B is the buoyancy parameter defined respectively as:

$$Ca=0.5\frac{\rho C_D b_v U^2 l_v^3}{EI} \tag{3b}$$

$$B=\frac{(\rho-\rho_v)g b_v t_v l_v^3}{EI} \tag{3c}$$

with I the second moment of area ($=b_v t_v^3/12$ for a rectangular section), t_v the blade thickness, E the elastic modulus, and ρ_v the vegetation tissue density. In Luhar and Nepf (2011) the in-canopy velocity magnitude U is vertically uniform, while in the present model U varies over depth ($U=\sqrt{u^2+v^2}$). The actual implementation of the model is subject to verification through the bending angle from vertical of the deflected canopy (Luhar and Nepf, 2011):

$$\theta=\cos^{-1}\left(\frac{l_{ve}}{l_v}\right)^{1/3} \tag{3d}$$

The wave-induced streaming (oscillatory contribution to steady wave stress) in the direction of wave propagation within the vegetation canopy (observed by Luhar et al., 2010; Luhar and Nepf, 2013) is implemented in the momentum balance as an additional wave-averaged forcing (similar to streaming in the wave boundary layer) as:

$$F_{s,\ veg}=\frac{S_{d,\ veg,\ tot}\tilde{k}}{\rho_0\tilde{\sigma}} \tag{4}$$

where $\tilde{k}$ is the mean wave number, $\tilde{\sigma}$ is the mean wave frequency, and $S_{d,veg,tot}$ is the total wave energy dissipation due to vegetation term calculated in the wave model (Eq. (10)) and exchanged with the flow model.

The vertical Reynolds stresses (vertical flux of horizontal momentum by turbulent velocity fluctuations) are related to the mean flow through the use of an eddy viscosity:

$$\overline{u'w'}=-K_M\frac{\partial u}{\partial z} \tag{5a}$$

$$\overline{v'w'}=-K_M\frac{\partial v}{\partial z} \tag{5b}$$

where the overbar represents a time average and the prime represents a fluctuation about the mean, and K_M is the eddy viscosity that is parameterized as:

$$K_M=c_\mu k^{1/2} l+\nu \tag{5c}$$

where k is the turbulent kinetic energy, l is a turbulent length scale (size of the largest turbulent eddies), and c_μ is a stratification stability function (for non-stratified or neutral flow $c_\mu=c_\mu^0\approx 0.55$). The variables k and l are computed with a generic (GLS) two-equation turbulence model (Umlauf and Burchard, 2003 in Warner et al., 2005) that can represent several classic turbulence model schemes (e.g., $k-kl$, $k-\varepsilon$, and $k-\omega$):

$$\frac{\partial k}{\partial t}+\vec{v}\bullet\nabla k=\frac{\partial}{\partial z}\left(\frac{K_M}{\sigma_k}\frac{\partial k}{\partial z}\right)+P_s+P_{veg}+B-\varepsilon \tag{6a}$$

where σ_k is the turbulent Schmidt number for k, P_s is the production of k by shear, P_{veg} is the production of k by vegetation (see Eq. (7)), B is the buoyancy flux, and ε is the turbulent dissipation expressed as:

$$\varepsilon=(c_\mu^0)^{3+p/n}k^{3/2+m/n}\psi^{-1/n} \tag{6b}$$

where (p, n, m) is a set of parameters to retrieve the classic turbulence models (Table 1 in Warner et al., 2005), and $\psi=(c_\mu^0)^p k^m l^n$ is the generic parameter satisfying the second equation of the turbulence model:

$$\frac{\partial \psi}{\partial t}+\vec{v}\bullet\nabla\psi=\frac{\partial}{\partial z}\left(\frac{K_M}{\sigma_\psi}\frac{\partial \psi}{\partial z}\right)+\frac{\psi}{k}(c_1 P+c_3 B-c_2\varepsilon F_{wall}-D_{veg}) \tag{6c}$$

where σ_ψ is the turbulent Schmidt number for ψ, c_1 and c_2 are coefficients selected to be consistent with the von Karman constant and with experimental observations for decaying homogeneous isotropic turbulence (Wilcox, 1998 in Warner et al., 2005), c_3 is a coefficient depending on stratification stability, F_{wall} is a wall proximity function, and D_{veg} is an extra dissipation term due to vegetation (see Eq. (8)).

According to Uittenbogaard (2003), the turbulence production due to vegetation in Eq. (6a) is expressed as:

$$P_{veg}=\sqrt{(F_{d,\ veg,u}u)^2+(F_{d,\ veg,v}v)^2} \tag{7}$$

and the source of enstrophy or dissipation due to vegetation in Eq. (6c) is expressed as:

$$D_{veg}=c_2\frac{P_{veg}}{\tau_{eff}} \tag{8a}$$

with τ_{eff} defined as the minimum between the dissipation time scale of free turbulence and the dissipation time scale of eddies in between the plants:

$$\tau_{eff}=\min(\tau_{free},\tau_{veg}) \tag{8b}$$

where,

$$\tau_{free}=\frac{k}{\varepsilon} \tag{8c}$$

and

$$\tau_{veg}=\left(\frac{L^2}{c_k^2 P_{veg}}\right)^{1/3} \tag{8d}$$

with $c_k=(c_\mu^0)^4\simeq 0.09$ and L is the typical length scale between the plants defined as:

$$L(z)=c_l\left(\frac{1-b_v t_v n_v}{n_v}\right)^{1/2} \tag{8e}$$

with c_l a coefficient of order unity.

The stress exerted on the flow by the bed is calculated using a quadratic drag coefficient and assuming a logarithmic profile in the bottom cell (Warner et al., 2008a, 2008b). The presence of waves increases bottom mixing which affects the bottom resistance experienced by a current, and can be interpreted as an apparent increase in the bottom roughness (Madsen, 1994).

2.2. Wave model

SWAN (Simulating Waves Nearshore) is a third-generation spectral wave model based on the action balance equation (Booij et al., 1999):

$$\frac{\partial N}{\partial t}+\frac{\partial c_x N}{\partial x}+\frac{\partial c_y N}{\partial y}+\frac{\partial c_\sigma N}{\partial \sigma}+\frac{\partial c_\theta N}{\partial \theta}=\frac{S_{tot}}{\sigma} \tag{9}$$

N being the action density defined as the ratio of the wave energy density (or variance spectrum) distributed over (intrinsic) wave frequency (σ) and direction of propagation (θ) divided by frequency ($=E(\sigma,\theta)/\sigma$), where c is the propagation velocity. The equation is a balance between local rate of change, advection in the horizontal (x and

y) directions, shifting of relative frequency due to variation in water depth and current (exchanged between the flow and wave models), depth-induced refraction and additional source/sink terms (S_{tot}), namely wave-growth due to wind input, energy transfer due to wave-wave interactions, and dissipation due to white-capping, depth-induced breaking, and bottom friction (plus vegetation drag described in next paragraph). SWAN can also account for diffraction, partial transmission, and reflection.

Wave dissipation due to vegetation is computed with the formulation of Mendez and Losada (2004) following the work of Dalrymple et al. (1984) on cylinders, which was implemented in SWAN by Suzuki et al. (2012) as:

$$S_{d,\ veg}=-\sqrt{\frac{2}{\pi}}g^2\widetilde{C_D}b_v n_v\left(\frac{\tilde{k}}{\tilde{\sigma}}\right)^3\frac{sinh^3(\tilde{k}l_v)+3sinh(\tilde{k}l_v)}{3\tilde{k}cosh^3(\tilde{k}h)}\sqrt{E_{tot}}E(\sigma,\theta) \quad (10)$$

where $\widetilde{C_D}$ is a bulk drag coefficient (that may be dependent on the Keulegan-Carpenter number $K_C=u_c T_p/b_v$ with u_c a characteristic velocity acting on the plants, and T_p the wave period), $\tilde{k}$ is the mean wave number, $\tilde{\sigma}$ is the mean wave frequency, h is the water depth, E_{tot} is the total wave energy, and E is the wave energy at frequency σ and direction θ. This term was derived neglecting the shearing generated at the top of the canopy, and the inertial force caused by the fluid accelerating past the plant stems (Morison et al., 1950). However, Luhar et al. (2010) underline that the inertia-dominated regime (when the wave orbital excursion is much smaller than the drag and shear length scales) is not relevant for field conditions, and that the energetic contribution of the work done by the shear stress is typically two order of magnitude smaller than the energy dissipation due to the drag. In the present version of SWAN, the vegetation height l_v cannot vary spatially, and therefore the effect of plant reconfiguration under current-forcing on wave dissipation is not currently accounted for.

2.3. Test case configuration

The implementation of the wave-flow-vegetation interactions were evaluated in the COAWST modeling system with an application to an idealized model domain that represents a 10 km by 10 km and 1 m deep basin. The model is forced by oscillating the water level on the northern edge with a tidal amplitude of 0.5 m and a period of 12 h. Waves are also imposed on the northern edge with a height of 0.5 m, directed to the south (zero angle), with a period of 2 s. The southern edge of the model domain is closed (zero gradient condition for the surface elevation and the tangential velocity components, and normal velocity components set to zero). The (western and eastern) sides have a zero gradient boundary condition for the flow and an absorbing condition for the wave energy. A square patch of vegetation (1 km by 1 km) is placed in the middle of the domain. The selected vegetation type is submerged and designed to resemble eelgrass (*Zostera marina*). The plant stems are 30 cm high, 0.3 cm wide, and (if flexible) thickness is set to 0.3 mm thick, mass density to 700 kg/m^3 and elastic modulus to 1 GPa (Luhar and Nepf, 2011; J. Testa, pers. comm.). The drag coefficients in the flow model (C_D) and in the wave model ($\widetilde{C_D}$) are set to 1 (typical value for a cylinder at high Reynolds number). The density is set to 2500 stems/m^2 (packing density a=7.5 m^{-1}) which is a dense vegetation canopy according to Ghisalberti and Nepf (2004) and Nepf (2012). The bed roughness is z_0=0.05 mm which corresponds to a mixture of silt and sand (Soulsby, 1997). The turbulence model selected is the $k-\varepsilon$ scheme. The grid is 100 by 100 in the horizontal (100 m resolution) and has 40 vertical sigma-layers (uniformly distributed). The ROMS barotropic and baroclinic time steps are respectively 0.05 s and 1 s, while the SWAN time step and the coupling interval between ROMS and SWAN are 10 min.

Several scenarios were simulated to evaluate the hydrodynamic effects of vegetation (Table 1): (1) NV: non-vegetative cases or control experiments in which the vegetation module is not activated; (2) T: the flow model alone with (stiff or flexible) vegetation drag and turbulence mixing; (3) W: the wave model alone with wave energy dissipation due to stiff vegetation; (4) WC: the wave and flow models coupled but no free surface elevation fields from the flow model to the wave model (option *ZETA_CONST*); (5) WWL: flow model and wave model coupled but no current fields from the flow model to the wave model (option *UV_CONST*); (6) FW: full coupling of the flow and wave models.

Table 1
Model scenarios analyzed in the paper.

Model scenario	Forcing/processes	Paper section
NV	tide and/or waves, no vegetation	3.2, 3.3, 3.4, 3.5
T	tide only	3.1, 3.2
W	waves only	3.3
WC	waves and tidal currents	3.4.1
WWL	waves and tidal water level fluctuations	3.4.2
FW	tidal flow and waves	3.5

3. Results

3.1. Model verification

Different components of the model have already been validated against multiple sets of laboratory experiments with rigid vegetation: drag force (Eq. (2)) and turbulent vertical mixing (Eqs. (7)-(8)) by Uittenbogaard (2003), and wave dissipation (Eq. (10)) by Suzuki et al. (2012). Here, we focus on the current-vegetation interaction parameterization using an effective blade length (Eq. (3)) to account for plant reconfiguration when predicting the drag force by flexible vegetation. The deflected canopy height (l_d) is located at the point of inflection in the vertical velocity profiles (Fig. 1) either simulated by the test case or measured in and above real eelgrass canopies by Lacy and Wyllie-Echeverria (2011) at different phases of the tide. The bending of the blade simulated and measured in the field ($\theta=\cos^{-1}(l_d/l_v)$) are compared to the values obtained from Eq. 3d by normalizing the velocity at the top of the canopy through a Froude number ($Fr=U/\sqrt{gl_v}$) (Fig. 3). The simulated and the observed bending angles comply with the semi-empirical model, confirming the validity of the effective blade length expression of Luhar and Nepf (2011) and its implementation in COAWST.

A parameterization of wave-induced streaming by vegetation (analogous to viscous boundary streaming) has been implemented but remains to be verified against laboratory and field measurements (Luhar et al., 2010 and Luhar and Nepf, 2013, respectively). The present case study was not appropriate for investigating this process as most of the wave dissipation by vegetation occurred only locally at the edge of the vegetation patch. A configuration with additional wind-wave generation over the entire model domain could provide more similar wave conditions to the investigations of in-canopy wave-induced streaming cited above.

The results of the few observations on wave attenuation by vegetation in presence of different flow conditions (e.g., Paul et al., 2012; Maza et al., 2015) highlight the strong nonlinearities among waves, currents and vegetation. Rather than trying to match the experimental setup to be able to verify the model, the present study (following sections) uses the model as a tool to qualitatively investigate the different processes involved in wave-current-vegetation interactions.

3.2. Effects of vegetation on tidal flow

In this section, we consider tidal flow in the absence of waves (scenario T), and focus on a snapshot at peak flood defined as the instant of maximum velocity in the middle of the domain. The drag exerted by vegetation reduces the mean flow compared to non-

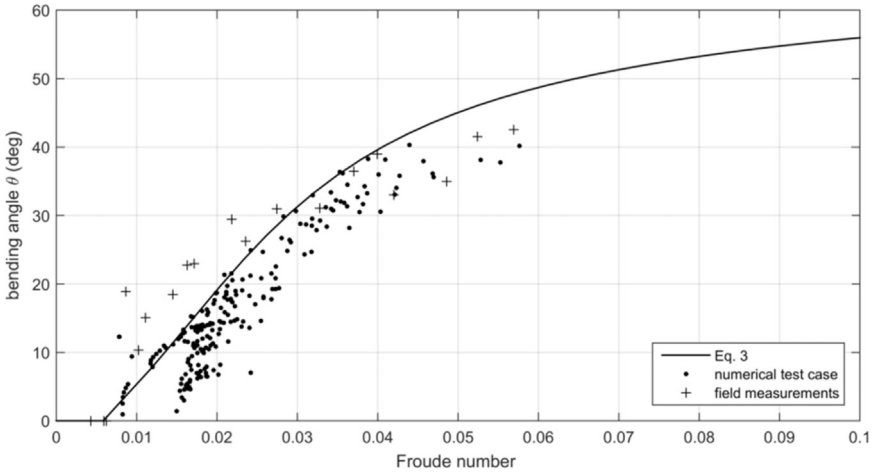

Fig. 3. Bending angle from vertical plotted against the Froude number calculated at the top of the canopy taken as the height of the inflection point in the velocity profiles either simulated by the test case at different phases of the tide (dot) or measured in the field (cross) by Lacy and Wyllie-Echeverria (2011), superimposed on the semi-empirical model (solid line) of Luhar and Nepf (2011) assuming uniform in-canopy flow velocity.

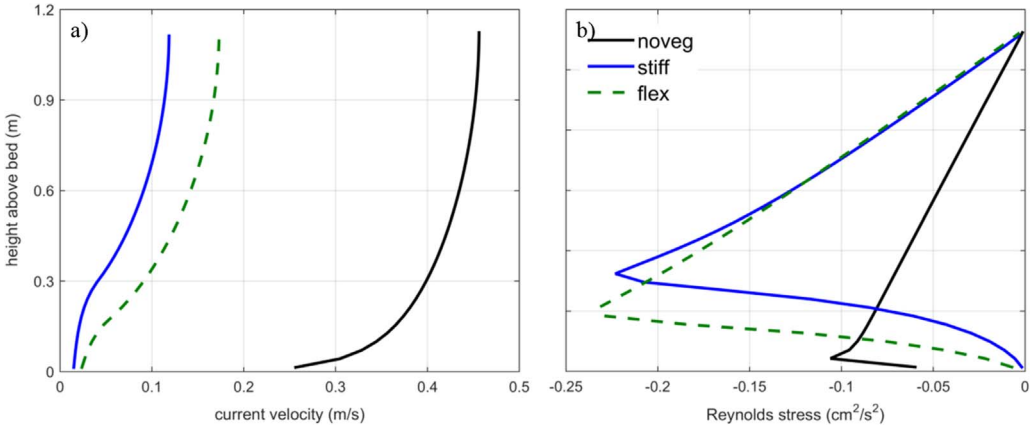

Fig. 4. Vertical profiles of a) mean flow velocity, and b) turbulent Reynolds shear stress ($\overline{v'w'}=-K_M\frac{\delta v}{\delta z}$) in the middle of the patch at peak flood without vegetation (solid black), with stiff vegetation (solid blue), and with flexible vegetation (dash green). (For interpretation of the references to color in this figure legend, the reader is referred to the web version of this article.)

vegetated (or bare) bed. The flow structure displays an S-shape with an inflection point near the top of the canopy (Fig. 4a). In addition to affecting the mean flow velocity, vegetation also affects the turbulence intensity and mixing. Turbulent shear stress is generated by the drag discontinuity across the canopy interface, and peaks near the top of the canopy (Fig. 4b). As opposed to the theoretical mixing layer (hyperbolic tangent velocity profile) and the vegetation shear layer described in Ghisalberti and Nepf (2004, 2006), the present vegetation shear layer has no clear limits as it is embedded within the tidal boundary layer (linear Reynolds stress profile). Within the canopy, shear-scale turbulence is dissipated and wake-scale turbulence is generated. A simulation leaving out the additional vegetative turbulence terms (Eqs. (7)-(8)) shows that wake-generated turbulence contributes to about 50% of the total turbulence in accordance with the measurements of Nepf and Vivoni (2000), and reduces the vertical velocity gradient by 25% on average in the patch (not shown). Because the flexible vegetation is bent over by the current, the drag is reduced, but the canopy shear layer is lower in the water column, so the bed experiences more stress (Fig. 4b).

The drag exerted by vegetation leads to a change in water level. Overall, the vegetative drag force is balanced by a pressure gradient (Fig. 5a). In the canopy, the vegetative drag force is mostly balanced with the turbulent stress with smaller contribution from the pressure gradient as opposed to the overlying part of the water column (Fig. 5b). The adjustment of the water level around the patch (set-up upstream and set-down downstream) is linked to a modification of the flow, decelerating upstream and in the wake of the patch, while accelerating at the edges (Fig. 6). In the case of rigid vegetation, the patch induces a water level change of 20% (relative difference with the non-vegetative case), a reduction of the depth-averaged velocity in the patch and directly in its wake of 80%, and an increase of the depth-averaged velocity at the edge of the patch (elongated lobes in the direction of the flow) of 40%.

3.3. Effects of vegetation on wave characteristics and wave-induced flow

In this section, we consider waves only, in the absence of tidal flow (scenario W). The 0.5 m and 2 s waves forced at the northern boundary adjust quickly due to breaking, white-capping, and bed friction. At the vegetation patch the significant wave height (defined as the mean wave height of the highest third of the waves) is already reduced by a factor 5. The best-fit exponential decay coefficient (Lacy and MacVean, 2016) characterizing wave dissipation in this portion of the domain is $\alpha=3.2\cdot10^{-4}\ m^{-1}$. Nevertheless, vegetation plays an important role in wave dissipation. The significant wave height is reduced to 5% of the non-vegetative case value in and directly behind the patch (Fig. 7a). The exponential decay coefficient characterizing wave dissipation due to vegetation drag is $\alpha=3.9\cdot10^{-3}\ m^{-1}$ (an order of magnitude larger than bed friction). The peak period is unchanged but the mean wave period

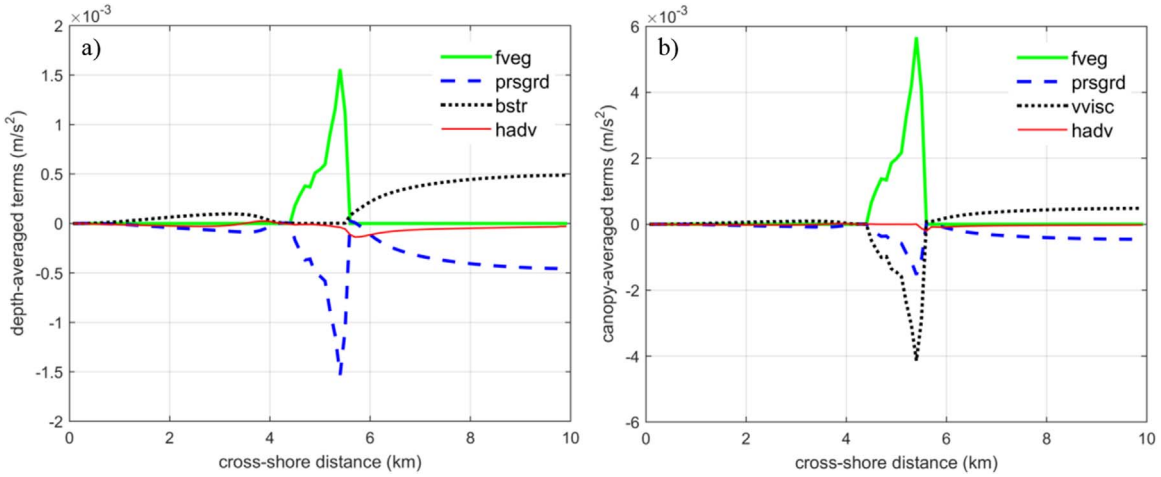

Fig. 5. Cross-shore (along Y-axis) variation of momentum balance terms integrated over a) the water column and b) the canopy, in the middle of the domain in the case of stiff vegetation (fveg=vegetation drag, prsgrd=pressure gradient, bstr=bottom friction, vvisc=vertical viscosity, hadv=horizontal advection). Wave propagation is from the right of the figure to the left of the figure.

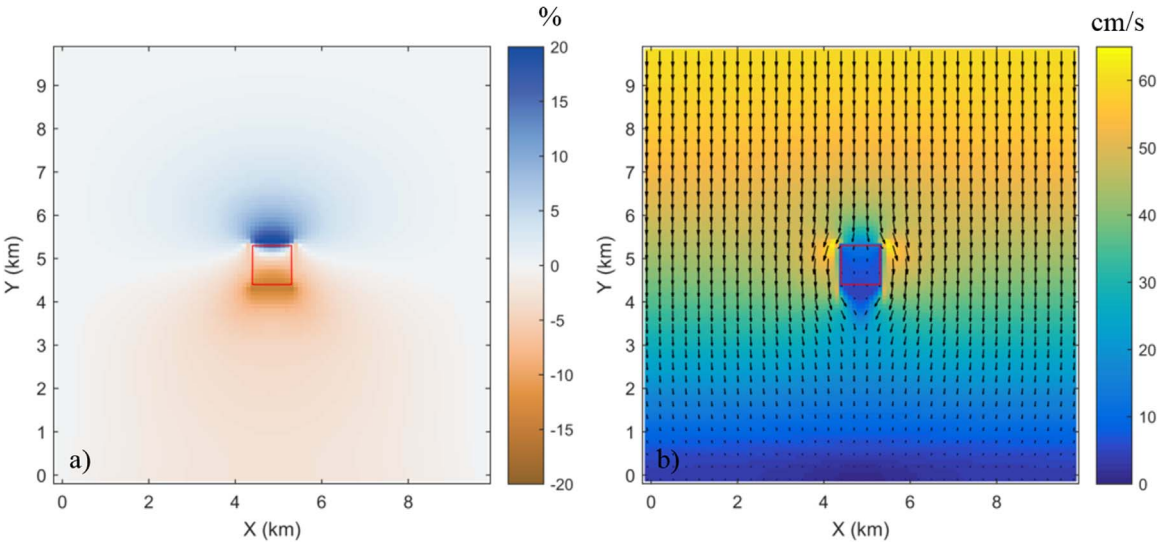

Fig. 6. Plan view of a) water level anomaly (relative difference between the stiff vegetation and the non-vegetation cases) and b) depth-averaged velocity, at peak flood. The patch of (stiff) vegetation is located in the red square. The hydrodynamic is forced at the northern boundary.

increases up to 10% (Fig. 7b) and the mean wave length increases up to 15% (Fig. 7c). This reduction in wave height and increase in wave length result in a reduction of wave steepness (Fig. 7d), so the vegetation tends to smooth the sea surface locally and behind the patch (glassy appearance observed in the field). As a corollary of wave dissipation, the presence of a vegetation patch induces sharp horizontal variations in wave height responsible for wave directional spreading (diffraction effect).

As the wave energy (and momentum) flux decreases due to bottom friction, the mean water level increases (setup) to balance. The patch of vegetation dampens the wave-driven flow resulting in an additional wave setup (Fig. 8a). Interestingly, the convergence of wave energy flux behind the vegetation patch generates an area of enhanced current (Fig. 8b). The magnitude of the wave-driven flow is much smaller than the tidal flow in this case, nevertheless these results give a sense of the qualitative influence of vegetation in wave-dominated environments.

3.4. *Effects of vegetation-influenced tidal flow on wave characteristics*

Tides influence wave characteristics by varying both current and water depth. To isolate these two processes, we analyze sequentially the outputs of two wave model runs: one with no water level fluctuation (scenario WC) and the other with the current set to zero (scenario WWL).

3.4.1. *Effects of vegetation-influenced currents on wave characteristics*

In this section, we analyze the effects of currents on waves, in the absence of water level fluctuations (scenario WC). Overall, the waves are bigger during flood tide than during ebb tide as the rate of wave energy dissipation is reduced with a following (flood) current and increased with an opposing (ebb) current (Figs. 9–10). This applies to wave dissipation due to vegetation, reduced by 40% at flood and increased by a factor two at ebb relative to the non-tidal case (Fig. 9b). Nevertheless, the significant wave height in the vegetation patch is smaller with flood current than with no current (Fig. 9a). It appeared that the intrinsic/relative wave period is also reduced at flood (increased at ebb, not shown) forcing the wave height to decrease to conserve wave action density. This result agrees with Bacchi et al. (2014) who indicated that the damping by vegetation is more important at higher wave frequencies. In addition, the apparent (absolute) wave period is also reduced at flood and increased at ebb as a result of Doppler shift; the vegetation patch damps the current and therefore attenuates this relativistic process: absolute and relative wave

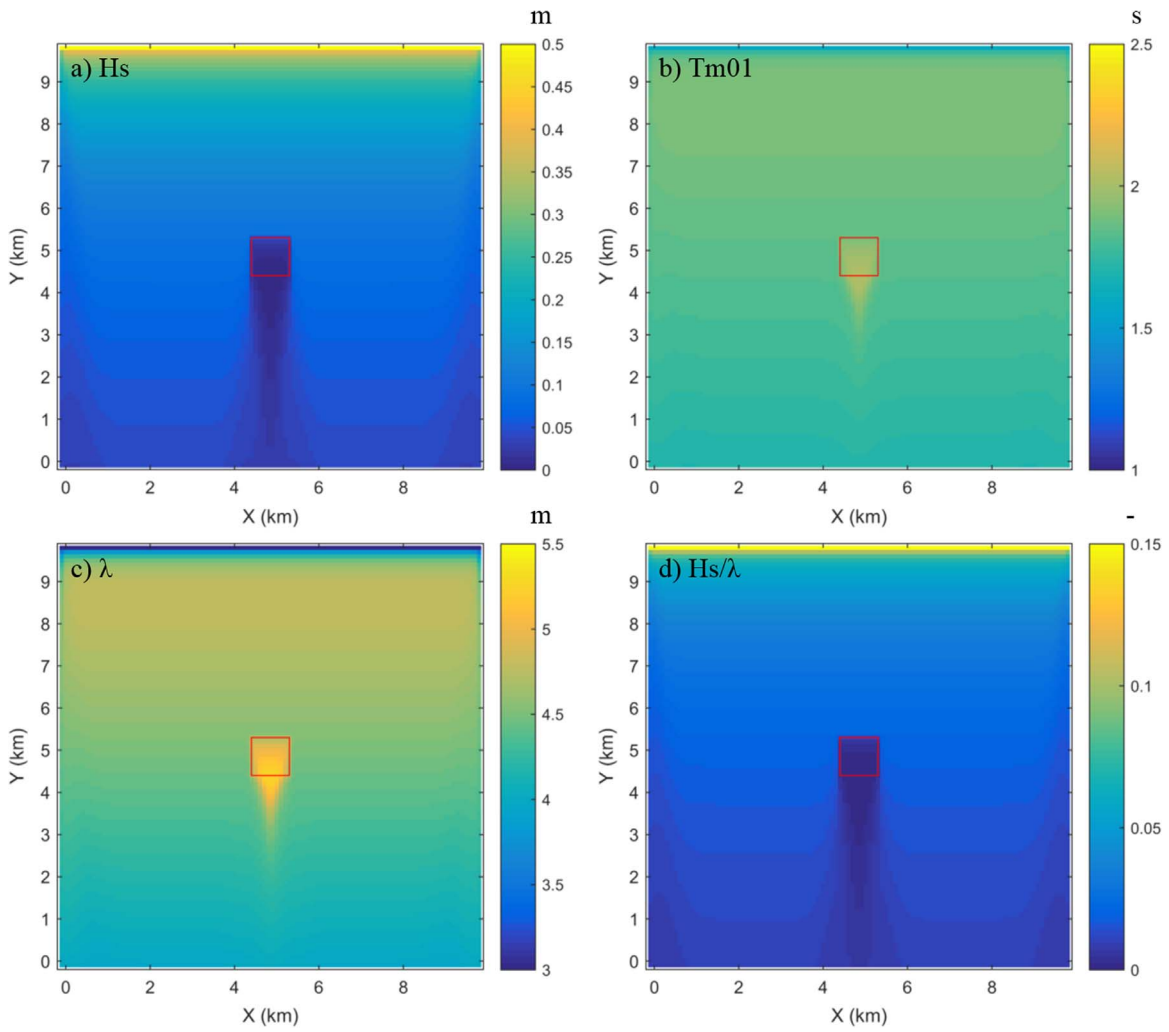

Fig. 7. Plan view of a) significant wave height Hs, b) mean wave period Tm01, c) mean wave length λ, and d) wave steepness Hs/λ.

periods are almost the same in the patch (higher at ebb than at flood). In addition to frequency shifting, the currents circulating around the vegetation patch induce wave refraction: the wave energy is focused at flood and obstructed at ebb (Fig. 10), which results in a more elongated wake at flood than at ebb.

3.4.2. Effects of vegetation-influenced water level on wave characteristics

In this section, we analyze the influence of water level on waves, in the absence of currents (scenario WWL). Overall, an increase in water level results in an increase of wave height and wave length, and vice versa in the case of a decrease in water level. The positive water level

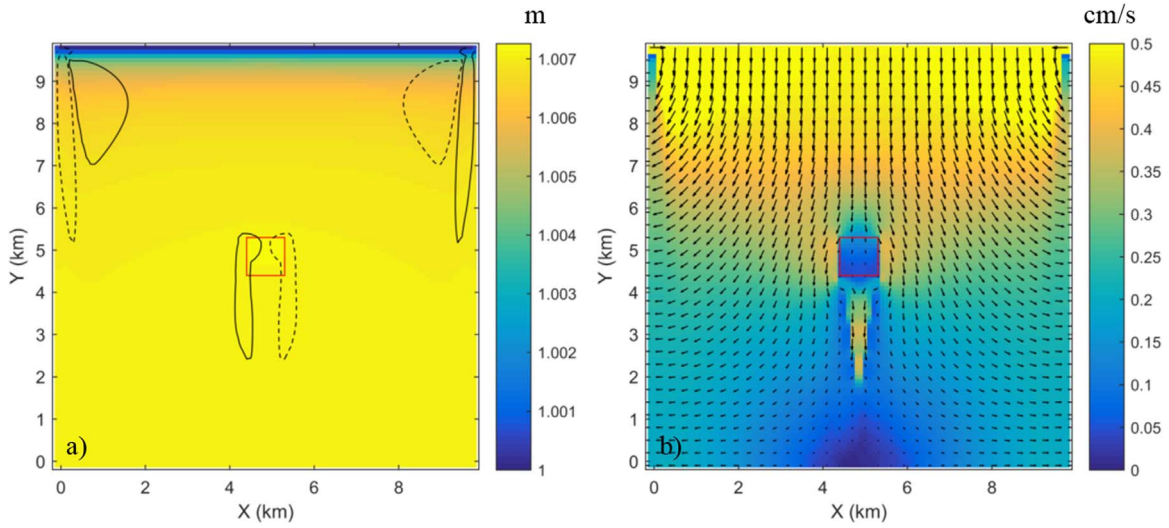

Fig. 8. Plan view of a) wave-induced mean water elevation in which the gradient contour levels −5e-6 (dash) and 5e-6 (solid) are superimposed and b) time- and depth-averaged Lagrangian current velocity. Note difference of magnitude in color scale from Fig. 6b (instantaneous currents).

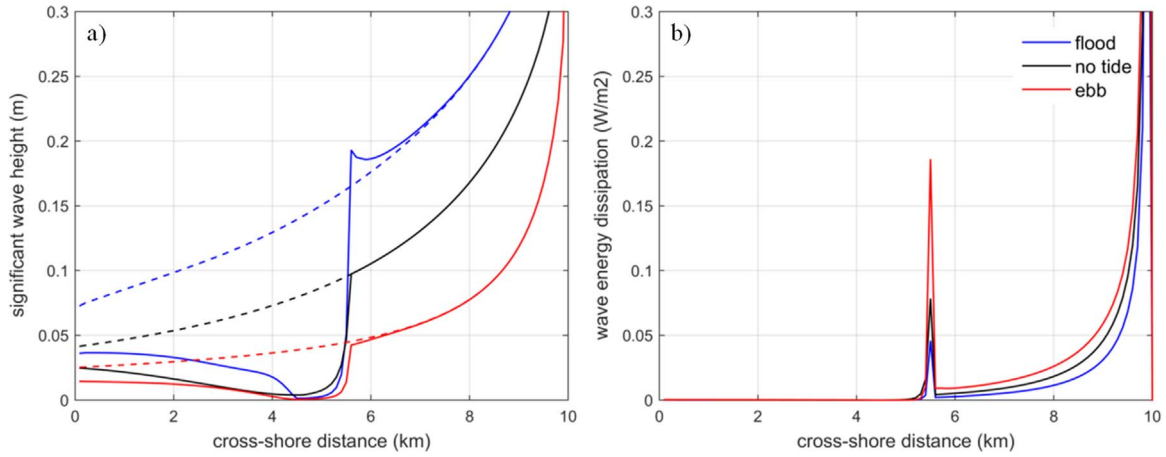

Fig. 9. Cross-shore (along Y-axis) variation of a) significant wave height and b) total wave energy dissipation in the middle of the domain at peak flood (blue), peak ebb (red), and with no tide (black). In the left panel, the dash lines are the results without vegetation. Wave propagation is from the right of the figure to the left of the figure. (For interpretation of the references to color in this figure legend, the reader is referred to the web version of this article.)

anomaly upstream of the vegetation patch (Fig. 6a) allows the presence of larger waves locally, and in the wake of the patch after propagation (Fig. 11a). For an opposite water level anomaly (down upstream and up downstream), the waves are smaller when they meet the patch, but they are enhanced (compared to the constant water level case) in the wake of the patch as a result of being less dampened in the patch (Fig. 11b).

3.5. Effects of vegetation-influenced waves on tidal flow

In this section, we analyze the influence of waves on tidal flow (scenario FW). The contribution of wave-forcing to the momentum balance is negligible at flood in the cross-section shown in Fig. 5 (two orders of magnitude less) but is manifest (10–20% increase in depth-averaged velocity) at the edge of the vegetation patch where the wave-induced Stokes flow interacts with strong flow vorticity, and as a result the lobes of maximum current velocity (Fig. 6b) are slightly shifted and more elongated in the direction of wave propagation. While flow speed increases on the lateral edges of the vegetation patch, it decreases upstream by ~ 20%, above the vegetation patch by ~ 75%, and in the v-shaped wave wake downstream by ~ 35%. In the tide-only case (Fig. 6b), the flow speed was reduced by ~ 10, 80 and 20%, respectively across the vegetation patch. Therefore, the capacity of vegetation to reduce the flow speed is enhanced in the presence of waves.

4. Discussion

4.1. Advancement of open-source modeling tools

Coastal storms are generally a combination of extreme water levels, strong winds, large waves, and intense rainfall. The simulation of these events require accounting for wind-wave-current interactions. The Coupled Ocean-Atmosphere-Wave-Sediment Transport (COAWST) modeling system has been successfully applied under various storm conditions in several coastal and estuarine environments (e.g., Warner et al., 2010, Olabarrieta et al., 2011, Ralston et al., 2013). The wave-flow-vegetation module now allows for quantification of the effects of emergent and submerged aquatic vegetation on storm surge, waves, and sediment transport, which can be used to inform ecosystem-based coastal risk management.

COAWST also integrates a coupled biogeochemical-optical model based on a nutrient, phytoplankton, zooplankton, and detritus model (Fennel et al., 2006) and a light attenuation model depending on concentrations of suspended sediment, organic material, and phytoplankton (del Barrio et al., 2014). The wave-flow-vegetation module provides a new linkage for assessing the hydrodynamic forces on a seagrass bed and the resulting sediment resuspension and mixing in and above the seagrass canopy that affect light availability, and in turn potential seagrass biomass production. Future versions of the code will

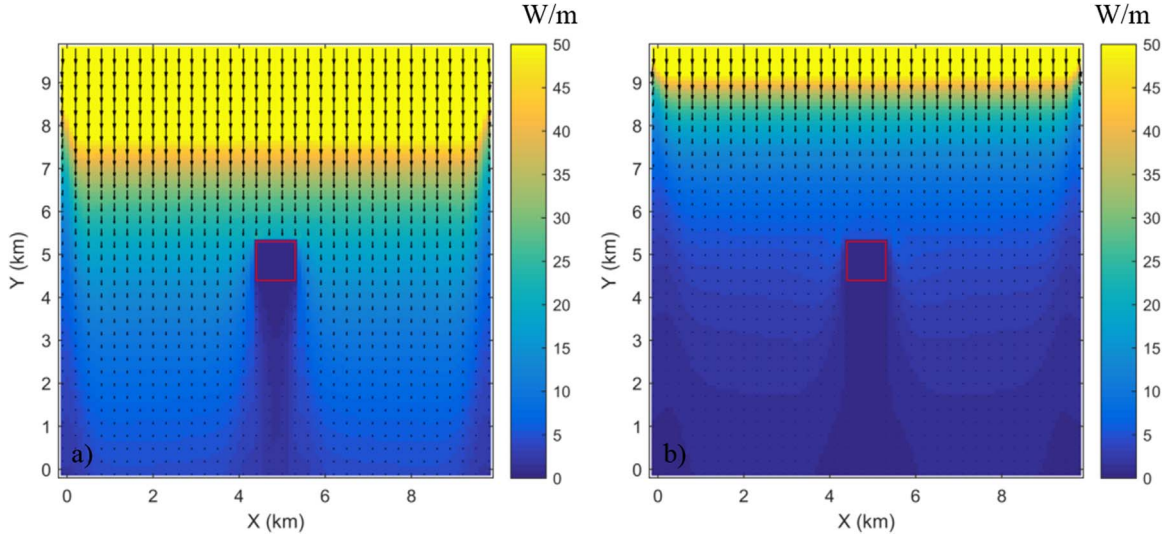

Fig. 10. Transport of wave energy during a) flood and b) ebb tides.

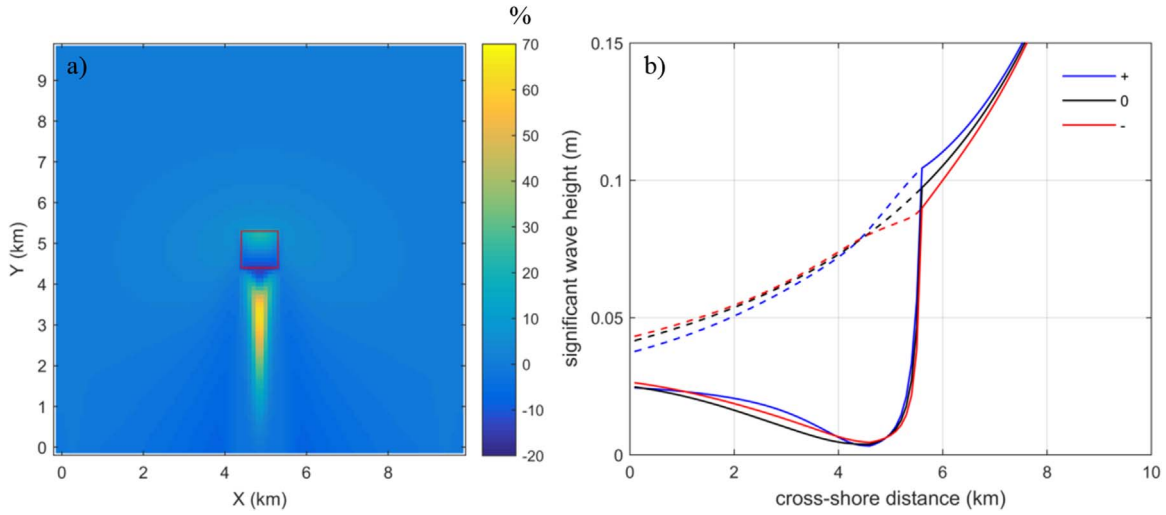

Fig. 11. a) Relative difference in significant wave height between the positive anomaly case (described in Fig. 6a) and the constant water level case, and b) cross-shore (along Y-axis) variation of significant wave height (in the middle of the domain) with a positive water level anomaly (blue), no anomaly (constant water level, black), and a negative anomaly (red). The dash lines are the results with no wave dissipation due to vegetation. (For interpretation of the references to color in this figure legend, the reader is referred to the web version of this article.)

include above and below ground biomass changes to vegetation classes based on light and nutrient availability.

4.2. Limitations and possible improvements

4.2.1. Calculation of bed shear-stress

The assumption of a logarithmic velocity profile near the bed is questionable within the vegetation canopy as is the calculation of bed shear-stress. In particular, the model in its current state cannot represent the enhanced bed shear-stress in sparse canopy compared to bare sediment that results in "sandification" (winnowing of mud) of the vegetated bed (Van Katwijk et al., 2010; Nepf, 2012). In addition to bed shear-stress partitioning to isolate the skin friction relevant to sediment transport, the calculation of the total bed shear-stress (drag form plus skin friction) should account for the contribution of the canopy shear-stress and wake-generated turbulence. Although the near-bed turbulent structure can be difficult to resolve with the vertical resolution used in coastal models, using the near-bed Reynolds stress (or the turbulent kinetic energy) instead of the vertical velocity gradient to calculate the total bed shear-stress could reproduce the density/flexibility dependent trend in bed shear-stress (Fig. 4b). As currently formulated, the model will represent the tendency for vegetated areas to trap sediment and reduce effective settling velocity, which is an important bio-physical feedback in coastal systems.

4.2.2. Parameterization of flexible canopy motions

The waving motions of flexible canopies, called *monami* when following coherent eddies, decrease the amount of vertical momentum transfer by up to 40% compared to rigid canopies (Ghisalberti and Nepf, 2006). Several LES models have been designed to resolve the eddy structures in the vegetated shear layer and their coupling with the plant motions (e.g., Ikeda et al., 2001, Dupont et al., 2010), but to the authors' knowledge there is no existing eddy viscosity parameterization accounting for these interactions.

The wave dissipation due to vegetation term in SWAN currently neglects the plant swaying motion. Luhar and Nepf (2016) recently extended their effective blade length approach for steady-flow (Luhar and Nepf, 2011) to unsteady-flows, accounting for plant flexibility and motion in wave dissipation models. Their formulation will be implemented in COAWST along with expanding horizontally the dimension of the vegetation height variable in SWAN. Nevertheless, further investigations remain ongoing regarding the flexible plant reconfiguration under combined wave and current interactions.

4.2.3. Computational expense, obstacles and future considerations

We compared the computational costs of using the vegetation module relative to a simplified approach that uses bottom roughness to account for increased drag in the model domain. The increase in the computational costs arises in different parts of the model, mainly in the 2D and 3D kernels, and the GLS vertical mixing model which computes turbulent quantities (Table 2). Overall, the vegetation module increases computational costs by 6% over a run where the vegetation patch is represented by coarser sediment. The increase occurs from the calculation of the vegetation drag and turbulence terms in the vegetation module. These terms are then added to the 2D kernel, 3D momentum equations, and vertical mixing parameterization.

The implementation of this functionality in COAWST was met by several numerical and conceptual obstacles, which will require future investigation and troubleshooting. For example, the ROMS hydrodynamic model required a reduced time step with the vegetation module (e.g. 1 s instead of 10 s) to eliminate instabilities resulting from sharp velocity gradients. We also found that horizontal buoyancy and shear terms in the turbulence model needed to be unsmoothed to avoid perturbations at the corner of the vegetation patch. One possible solution is to gradually ramp up vegetation density into the patch, which can either be accomplished through modification of the initialization file, or through a coding modification. The SWAN model currently does not account for multiple vegetation types, and does not dissipate wave energy (due to vegetation) spectrally; i.e. dissipation is applied uniformly across the wave spectra. In the case of multiple

Table 2
Increase in computational expense due to implementation of the vegetation module relative as opposed to a simplified approach that uses bottom roughness to account for increased drag. All times are in seconds, summed over 24 cpus.

Model component	Bottom roughness case	Vegetation module case	Increase in computational time
Vegetation module	N/A	4310.716	N/A
2D kernel	108,442.567	113,364.426	4.53%
GLS vertical mixing	18,379.465	20,150.028	9.63%
3D kernel	62,767.183	63,416.523	1.03%
Total	192,294.957	203,947.535	6.14%

vegetation types an equivalent shoot density is defined in ROMS and SWAN. Future versions of SWAN will account for spatially-variable plant properties as in ROMS. Lastly, a systematic parameter study would constrain the uncertainty of the numerous model parameterizations implemented here. The development of this open-source tool will allow such studies to commence.

5. Summary and conclusion

We have developed a coupled wave-flow-vegetation module in the COAWST modeling system applicable to vegetated flows in riverine, lacustrine, estuarine and coastal environments. New vegetative components were implemented in the flow model ROMS, namely plant posture-dependent three-dimensional drag, vertical mixing, and wave-induced streaming. The model reproduces key features of flow-vegetation hydrodynamic interaction, in particular the strong shear layer at the top of a submerged canopy which varies in height as the plants bend. The coupling framework has also been updated to exchange vegetation-related variables between the flow and the wave model SWAN to account for wave dissipation by vegetation in the presence of currents and water level fluctuations. Results from the idealized test case in shallow water highlight the nonlinear interdependency between (tidal) flow and wave characteristics in the presence of a vegetation patch. In particular, the coupled wave-flow-vegetation model shows that the vegetation modifies the wave characteristics (height, period, steepness, and direction) primarily by wave energy dissipation resulting from the work done by drag force on the vegetation stems, and secondarily by influencing the water level and current fields: i) any (positive or negative) gradient of free surface elevation across the vegetation patch reduces vegetation-induced wave damping; ii) wave dissipation rate decreases/increases when waves propagate along/against the current, while the (intrinsic) wave frequency increases/decreases to conserve wave action density which enhances/diminishes wave dissipation by bed friction and vegetation drag. In parallel, waves influence the flow; therefore, waves alter the capacity of vegetation to reduce current speed and adjust water level. This model contributes to an improved understanding of how aquatic vegetation influences the physical environment and, more generally, provides a multidisciplinary tool for informing decision-making of the potential ecologic and economic benefits of aquatic vegetation.

Acknowledgment

This study was part of the Estuarine Physical Response to Storms project (GS2-2D), supported by the Department of Interior Hurricane Sandy Recovery program. This paper benefitted from discussions with Alfredo Aretxabaleta, Dan Nowacki and Heidi Nepf, and from the internal review of Jessica Lacy. The model in its current state (COAWST v3.2) is freely available (http://woodshole.er.usgs.gov/operations/modeling/COAWST/index.html) and model development is being conducted as an open-source community effort. We encourage feedback that will continue to add features and make the model more robust as the community of users and developers grows.

References

Bacchi, V., Gagnaire, E., Durand, N., Benoit, M., 2014. Wave energy dissipation in TOMAWAC. Telemac & Mascaret User Club, Grenoble, France, 15–17 Oct 2014.

Barbier, E.B., Koch, E.W., Silliman, B.R., Hacker, S.D., Wolanski, E., Primavera, J., Granek, E.F., Polasky, S., Aswani, S., Cramer, L.A., Stoms, D.M., Kennedy, C.J., Bael, D., Kappel, C.V., Perillo, G.M.E., Reed, D.J., 2008. Coastal ecosystem-based management with nonlinear ecological functions and values. Science 18, 321–323.

Booij, N., Ris, R.C., Holthuijsen, L.H., 1999. A third-generation wave model for coastal regions, Part I, model description and validation. J. Geophys. Res. C4 104, 7649–7666.

Carr, J., D'Odorico, P., McGlathery, K., Wiberg, P., 2010. Stability and bistability of seagrass ecosystems in shallow coastal lagoons: role of feedbacks with sediment resuspension and light attenuation. J. Geophys. Res. 115, G03011.

Chen, S.-N., Sanford, L., Koch, E.W., Shi, F., North, E.W., 2007. A nearshore model to investigate the effects of seagrass bed geometry on wave attenuation and suspended sediment transport. Estuaries Coasts 30 (2), 296–310.

Dalrymple, R.A., Kirby, J.T., Hwang, P.A., 1984. Wave diffraction due to areas of energy dissipation. J. Waterw. Port., Coast. Ocean Eng. 110, 67–79.

de Vriend, H.J., 2006. Integrated research results on hydrobiosedimentary processes in estuaries: algorithm for vegetation friction factor. Defra R & D Technical Report FD1905/TR3.

Dijkstra, J.T., Uittenbogaard, R.E., 2010. Modeling the interaction between flow and highly flexible aquatic vegetation. Water Resour. Res. 46, W12547.

DijkstraJ.T., 2012. Macrophytes in estuarine gradients: flow through flexible vegetation (Ph.D. thesis), TU Delft, 119 p.

Dupont, S., Gosselin, F., Py, C., De Langre, E., Hemon, P., Brunet, Y., 2010. Modelling waving crops using large-eddy simulation: comparison with experiments and a linear stability analysis. J. Fluid Mech. 652, 5–44.

Fennel, K., Wilkin, J., Levin, J., Moisan, J., O'Reilly, J., Haidvogel, D., 2006. Nitrogen cycling in the middle Atlantic Bight: results from a three-dimensional model and implications for the North Atlantic nitrogen budget. Glob. Biogeochem. Cycles 20, GB3007.

GanthyF., 2011. Rôle des herbiers de zostères (Zostera noltii) sur la dynamique sédimentaire du Bassin d'Arcachon. (Ph.D. thesis), University of Bordeaux, 284 p.

Ghisalberti, M., Nepf, H.M., 2004. The limited growth of vegetated shear layers. Water Resour. Res. 40, W07502.

Ghisalberti, M., Nepf, H.M., 2006. The structure of the shear layer in flows over rigid and flexible canopies. Environ. Fluid Mech. 6, 277–301.

Haidvogel, D.B., Arango, H.G., Budgell, W.P., Cornuelle, B.D., Curchitser, E., Di Lorenzo, E., Fennel, K., Geyer, W.R., Hermann, A.J., Lanerolle, L., Levin, J., McWilliams, J.C., Miller, A.J., Moore, A.M., Powell, T.M., Shchepetkin, A.F., Sherwood, C.R., Signell, R.P., Warner, J.C., Wilkin, J., 2008. Ocean forecasting in terrain-following coordinates: formulation and assessment of the regional ocean modeling system. J. Comput. Phys. 227 (7), 3595–3624.

Hemminga, M.A., Duarte, C.M., 2000. Seagrass Ecology. Cambridge University Press, Cambridge, UK.

Ikeda, S., Yamada, T., Toda, Y., 2001. Numerical study of turbulent flow and honami in and above flexible plant canopy. Int. J. Heat Fluid Flow 22, 252–258.

Jones, C.G., Lawton, J.H., Shachak, M., 1994. Organisms as ecosystem engineers. Oikos 69 (3), 373–386.

Kombiadou, K., Ganthy, F., Verney, R., Plus, M., Sottolichio, A., 2014. Modelling the effects of Zostera noltei meadows on sediment dynamics: application to the Arcachon lagoon. Ocean Dyn. 64, 1499–1516.

Kumar, N., Voulgaris, G., Warner, J.C., Olabarrieta, M., 2012. Implementation of the vortex force formalism in the coupled ocean-atmosphere-wave-sediment transport (COAWST) modeling system for inner shelf and surf zone applications. Ocean Model. 47, 65–95.

Lacy, J.R., Wyllie-Echeverria, S., 2011. The influence of current speed and vegetation density on flow structure in two macrotidal eelgrass canopies. Limnol. Oceanogr.: Fluids Environ. 1, 38–55.

Lacy, J.R., MacVean, L.J., 2016. Wave attenuation in the shallows of San Francisco Bay. Coast. Eng. 114, 159–168.

Lapetina, A., Sheng, Y.P., 2014. Three-dimensional modeling of storm surge and inundation including the effects of coastal vegetation. Estuar. Coasts 37, 1028–1040.

Lapetina, A., Sheng, Y.P., 2015. Simulating complex storm surge dynamics: three-dimensionality, vegetation effect, and onshore sediment transport. J. Geophys. Res. 120, 7363–7380.

Le Bouteiller, C., Venditti, J.G., 2014. Sediment transport and shear stress partitioning in a vegetated flow. Water Resour. Res. 51, 2901–2922.

Luhar, M., Coutu, S., Infantes, E., Fox, S., Nepf, H.M., 2010. Wave-induced velocities inside a model seagrass bed. J. Geophys. Res. 115, C12005.

Luhar, M., Nepf, H.M., 2011. Flow-induced reconfiguration of buoyant and flexible aquatic vegetation. Limnol. Oceanogr. 56 (6), 2003–2017.

Luhar, M., Nepf, H.M., 2013. From the blade scale to the reach scale: A characterization of aquatic vegetative drag. Adv. Water Res. 51, 305–316.

Luhar, M., Nepf, H.M., 2016. Wave-induced dynamics of flexible blades. J. Fluids Struct. 61, 20–41.

MadsenO.S., 1994. Spectral wave–current bottom boundary layer flows. In: Proceedings of the 24th International Conference on Coastal Engineering Research Council, Kobe, Japan, pp. 384–398.

Marjoribanks, T.I., Hardy, R.J., Lane, S.N., 2014. The hydraulic description of vegetated river channels: the weaknesses of existing formulations and emerging alternatives. WIREs Water 1, 549–560.

Maza, M., Lara, J.L., Losada, I.J., Ondiviela, B., Trinogga, J., Bouma, T.J., 2015. Large-scale 3-D experiments of wave and current interaction with real vegetation. Part 2: experimental analysis. Coast. Eng. 106, 73–86.

Mendez, F.M., Losada, I.J., 2004. An empirical model to estimate the propagation of random breaking and nonbreaking waves over vegetation fields. Coast. Eng. 51, 103–118.

Möller, I., Spencer, T., French, J.R., Legget, D.J., Dixon, M., 1999. Wave transformation over salt marshes: a field and numerical modeling study from Norfolk, England. Estuar. Coast. Shelf Sci. 49, 411–426.

Morin, J., M. Leclerc, M., Secretan, Y., Boudreau, P., 2000. Integrated two-dimensional macrophytes-hydrodynamic modelling. J. Hydraul. Res. 38, 163–172.

Morison, J.R., O'Brien, M.P., Johnson, J.W., Schaaf, S.A., 1950. The force exerted by surface waves on piles. Pet. Trans. AIME 189, 149–154.

Nepf, H.M., Vivoni, E.R., 2000. Flow structure in depth-limited, vegetated flow. J. Geophys. Res. 105 (C12), 547–557.

Nepf, H.M., 2012. Flow and transport in regions with aquatic vegetation. Annu. Rev.

Fluid Mech. 44, 123–142.
Olabarrieta, M., Warner, J.C., Kumar, N., 2011. Wave-current interaction in Willapa Bay. J. Geophys. Res. 116, C12014.
Paul, M., Bouma, T.J., Amos, C.L., 2012. Wave attenuation by submerged vegetation: combining the effect of organism traits and tidal current. Mar. Ecol. Prog. Ser. 444, 31–41.
Ralston, D.K., Warner, J.C., Geyer, W.R., Wall, G.R., 2013. Sediment transport due to extreme events: the Hudson River estuary after tropical storms Irene and Lee. Geophys. Res. Lett. 40, 5451–5455.
Ree, W.O., 1949. Hydraulic characteristics of vegetation for vegetated waterways. Agric. Eng. 30, 184–189.
Sheng, Y.P., Lapetina, A., Ma, G., 2012. The reduction of storm surge by vegetation canopies: three-dimensional simulations. Geophys. Res. Lett. 39 (20).
Soulsby, R.L., 1997. Dynamics of Marine Sands. Thomas Telford, London, 249.
Suzuki, T., Zijlema, M., Burger, B., Meijer, M.C., Narayan, S., 2012. Wave dissipation by vegetation with layer schematization in SWAN. Coast. Eng. 59 (1), 64–71.
Temmerman, S., Bouma, T.J., Govers, G., Wang, Z.B., De Vries, M.B., Herman, P.M.J., 2005. Impact of vegetation on flow routing and sedimentation patterns: three-dimensional modeling for a tidal marsh. J. Geophys. Res. 110, F04019.
Temmerman, S., Meire, P., Bouma, T.J., Herman, P.M.J., Ysebaert, T., de Vriend, H.J., 2013. Ecosystem-based coastal defence in the face of global change. Nature 504, 79–83.
Uittenbogaard R., 2003. Modelling turbulence in vegetated aquatic flows. International workshop on RIParian Forest vegetated channels: hydraulic, morphological and ecological aspects, Trento, Italy, 20–22 February 2003.
Umlauf, L., Burchard, H., 2003. A generic length-scale equation for geophysical turbulence models. J. Mar. Res. 61, 235–265.
Van Katwijk, M.M., Bos, A.R., Hermus, D.C.R., Suykerbuyk, W., 2010. Sediment modification by seagrass beds: muddification and sandification induced by plants cover and environmental conditions. Estuar. Coast. Shelf Sci. 89, 175–181.
Warner, J.C., Sherwood, C.R., Arango, H.G., Signell, R.P., 2005. Performance of four turbulence closure models implemented using a generic length scale method. Ocean Model. 8, 81–113.
Warner, J.C., Sherwood, C.R., Signell, R.P., Harris, C.K., Arango, H.G., 2008a. Development of a three-dimensional, regional, coupled wave. Curr. Sediment-Transp. Model. Comput. Geosci. 34, 1284–1306.
Warner, J.C., Perlin, N., Skyllingstad, E.D., 2008b. Using the model coupling Toolkit to couple earth system models. Environ. Model. Softw. 23, 1240–1249.
Warner, J.C., Armstrong, B., He, R., Zambon, J.B., 2010. Development of a coupled. Ocean Model. 35, 230–244.
Warner, J.C., Defne, Z., Haas, K., Arango, H.G., 2013. A wetting and drying scheme for ROMS. Comput. Geosci. 58, 54–61.
Wu, W., 2014. A 3-D phase-averaged model for shallow-water flow with waves in vegetated water. Ocean Dyn. 64, 1061–1071.